

Experimental study on thermal and mechanical properties of tailings-based cemented paste backfill with $\text{CaCl}_2 \cdot 6\text{H}_2\text{O}$ /expanded vermiculite shape stabilized phase change materials

Xiaoyan Zhang, Tianrun Cao, Lang Liu, Baoyun Bu, Yaping Ke, and Qiangqiang Du

Cite this article as:

Xiaoyan Zhang, Tianrun Cao, Lang Liu, Baoyun Bu, Yaping Ke, and Qiangqiang Du, Experimental study on thermal and mechanical properties of tailings-based cemented paste backfill with $\text{CaCl}_2 \cdot 6\text{H}_2\text{O}$ /expanded vermiculite shape stabilized phase change materials, *Int. J. Miner. Metall. Mater.*, 30(2023), No. 2, pp. 250-259. <https://doi.org/10.1007/s12613-022-2503-7>

View the article online at [SpringerLink](#) or [IJMMM Webpage](#).

Articles you may be interested in

Chang-sheng Yue, Ben Peng, Wei Tian, Guang-hua Lu, Gui-bo Qiu, and Mei Zhang, [Complete stabilization of severely As-contaminated soil by a simple \$\text{H}_2\text{O}_2\$ pre-oxidation method combined with non-toxic TMT-15 and \$\text{FeCl}_3 \cdot 6\text{H}_2\text{O}\$](#) , *Int. J. Miner. Metall. Mater.*, 26(2019), No. 9, pp. 1105-1112. <https://doi.org/10.1007/s12613-019-1819-4>

Qiu-song Chen, Shi-yuan Sun, Yi-kai Liu, Chong-chong Qi, Hui-bo Zhou, and Qin-li Zhang, [Immobilization and leaching characteristics of fluoride from phosphogypsum-based cemented paste backfill](#), *Int. J. Miner. Metall. Mater.*, 28(2021), No. 9, pp. 1440-1452. <https://doi.org/10.1007/s12613-021-2274-6>

Qian Zhou, Juan-hong Liu, Ai-xiang Wu, and Hong-jiang Wang, [Early-age strength property improvement and stability analysis of unclassified tailing paste backfill materials](#), *Int. J. Miner. Metall. Mater.*, 27(2020), No. 9, pp. 1191-1202. <https://doi.org/10.1007/s12613-020-1977-4>

Di Wu, Run-kang Zhao, Chao-wu Xie, and Shuai Liu, [Effect of curing humidity on performance of cemented paste backfill](#), *Int. J. Miner. Metall. Mater.*, 27(2020), No. 8, pp. 1046-1053. <https://doi.org/10.1007/s12613-020-1970-y>

Bo Wang, Chao-yi Chen, Jun-qi Li, Lin-zhu Wang, Yuan-pei Lan, and Shi-yu Wang, [Solid oxide membrane-assisted electrolytic reduction of \$\text{Cr}_2\text{O}_3\$ in molten \$\text{CaCl}_2\$](#) , *Int. J. Miner. Metall. Mater.*, 27(2020), No. 12, pp. 1626-1634. <https://doi.org/10.1007/s12613-020-2141-x>

Yu-ye Tan, Elmo Davide, Yu-cheng Zhou, Wei-dong Song, and Xiang Meng, [Long-term mechanical behavior and characteristics of cemented tailings backfill through impact loading](#), *Int. J. Miner. Metall. Mater.*, 27(2020), No. 2, pp. 140-151. <https://doi.org/10.1007/s12613-019-1878-6>



IJMMM WeChat



QQ author group

Experimental study on thermal and mechanical properties of tailings-based cemented paste backfill with $\text{CaCl}_2 \cdot 6\text{H}_2\text{O}$ /expanded vermiculite shape stabilized phase change materials

Xiaoyan Zhang¹⁾, Tianrun Cao¹⁾, Lang Liu^{1,2),✉}, Baoyun Bu¹⁾, Yaping Ke¹⁾, and Qiangqiang Du³⁾

1) Energy School, Xi'an University of Science and Technology, Xi'an 710054, China

2) Key Laboratory of Western Mines and Hazards Prevention, Ministry of Education of China, Xi'an 710054, China

3) School of Architecture and Civil Engineering, Xi'an University of Science and Technology, Xi'an 710054, China

(Received: 29 November 2021; revised: 15 April 2022; accepted: 18 April 2022)

Abstract: $\text{CaCl}_2 \cdot 6\text{H}_2\text{O}$ /expanded vermiculite shape stabilized phase change materials (CEV) was prepared by atmospheric impregnation method. Using gold mine tailings as aggregate of cemented paste backfill (CPB) material, the CPB with CEV added was prepared, and the specific heat capacity, thermal conductivity, and uniaxial compressive strength (UCS) of CPB with different cement–tailing ratios and CEV addition ratios were tested, the influence of the above variables on the thermal and mechanical properties of CPB was analyzed. The results show that the maximum encapsulation capacity of expanded vermiculite for $\text{CaCl}_2 \cdot 6\text{H}_2\text{O}$ is about 60%, and the melting and solidification enthalpies of CEV can reach 98.87 J/g and 97.56 J/g, respectively. For the CPB without CEV, the specific heat capacity, thermal conductivity, and UCS decrease with the decrease of cement–tailing ratio. For the CPB with CEV added, with the increase of CEV addition ratio, the specific heat capacity increases significantly, and the sensible heat storage capacity and latent heat storage capacity can be increased by at least 10.74% and 218.97% respectively after adding 12% CEV. However, the addition of CEV leads to the increase of pores, and the thermal conductivity and UCS both decrease with the increase of CEV addition. When cement–tailing ratio is 1:8 and 6%, 9%, and 12% of CEV are added, the 28-days UCS of CPB is less than 1 MPa. Considering the heat storage capacity and cost price of backfill, the recommended proportion scheme of CPB material presents cement–tailing ratio of 1:6 and 12% CEV, and the most recommended heat storage/release temperature cycle range of CPB with added CEV is from 20 to 40°C. This work can provide theoretical basis for the utilization of heat storage backfill in green mines.

Keywords: $\text{CaCl}_2 \cdot 6\text{H}_2\text{O}$ /expanded vermiculite; shape stabilized phase change materials; cemented paste backfill; thermal property; mechanical property

1. Introduction

With the resource exhaustion of surface and shallow mines, deep mining has become an essential key technology [1]. However, a large number of tailings and solid wastes will be produced in the process of deep mining. In addition, the two first-level indicators of comprehensive utilization of mine resources and energy saving and emission reduction occupy an important position in the latest “Green Mine Evaluation Indicators”, mainly including the disposal of solid waste and the utilization of geothermal resources [2–3]. The heat storage backfill technology is based on traditional cemented paste backfill (CPB), adding a certain proportion of shape stable phase change material (SSPCM) to replace some aggregates to form CPB with high heat storage capacity, this not only reuses solid wastes, but also can store the heat, which can be extracted for domestic hot water or air-conditioning equipment by pre-buried heat collection pipeline [4–6]. Therefore, it is crucial to clarify the properties of CPB

and SSPCM in the field of heat storage backfill technology.

The SSPCM is a kind of phase change medium between solid–solid and solid–liquid phase change materials (PCM), and it can keep PCM from leaking [7–8]. Porous carrier materials can absorb PCM because of their high specific surface area and abundant pore structure, such as expanded vermiculite [9], expanded perlite [10], diatomite [11], etc. Among them, the excellent porous layered structure of expanded vermiculite can ensure that PCM is well embedded in it by atmospheric impregnation method, and the preparation process is simple, which is more suitable for large-scale application in CPB [12]. However, the PCM absorbed in the porous carrier materials needs to meet the temperature conditions where the CPB is located. It is found that the mine resources with mining depth of 1000 m will face the surrounding rock temperature above 45°C [13–14]. The $\text{CaCl}_2 \cdot 6\text{H}_2\text{O}$ is preferred because of its lower price, suitable phase change temperature, and high thermal storage performance to meet the thermal storage cycle conditions of medium-deep mines [15].

✉ Corresponding author: Lang Liu E-mail: liulang@xust.edu.cn

© University of Science and Technology Beijing 2023

Therefore, it is necessary to study the application range of SSPCM in CPB.

At present, many scholars focused on the improvement and characteristics of CPB mechanical properties [16–22]. For example, Zhou *et al.* [17–18] studied the influence of underground mine water on the mechanical properties of CPB, and the results showed that the uniaxial compressive strength (UCS) of CPB would be rapidly reduced by soaking and drying–wetting cycle. Besides, it was also found that the mechanical properties of CPB could be greatly increased by adding 1% glass fibers with the length of 6 mm. Wang *et al.* [22] explored the mechanical properties of layered CPB with different structural characteristics based on cement–tailing ratio, and found that the mechanical properties of CPB decreased with the decrease of cement–tailing ratio. However, the heat storage/release performance of CPB is closely related to its own thermal properties, but there are few studies on the thermal properties of CPB at present. Because the material of CPB is similar to that of concrete in building industry, it is found that many scholars have studied the concrete added with SSPCM [23–30]. For example, Shen *et al.* [23] and Ren *et al.* [24] found that SSPCM can improve the heat storage capacity of concrete, but its thermal conductivity and UCS decreased significantly. Chen *et al.* [27] investigated that the particle size and addition amount of SSPCM have great influence on the internal temperature of concrete. Mohseni *et al.* [29] found that phase change concrete did not lose UCS after repeated thermal cycles, and the concrete added with SSPCM had good thermal stability. Zhu *et al.* [30] studied that the porosity of concrete with SSPCM was linearly related to water–cement ratio, and with the increase of SSPCM, the porosity of concrete with higher water–cement ratio increased more slowly than that of concrete with lower water–cement ratio.

The above literatures can provide the reference for adding SSPCM into CPB to improve its thermal property. More importantly, the mechanical and thermal properties of CPB with SSPCM are the basis for implementing heat storage backfill technology. However, there are few systematic studies on the adaptation of CPB with SSPCM to deep mine environment and the heat storage capacity of CPB in the phase change and non-phase change process of SSPCM. Based on the gaps of the above research, $\text{CaCl}_2 \cdot 6\text{H}_2\text{O}$ /expanded vermiculite shape stabilized phase change materials (CEV), which is easy to be industrialized, was prepared by atmospheric impregnation method, and CEV was added into the tailings-based CPB by direct addition method. The thermal and mechanical properties of CPB with different cement–tailing ratios and CEV addition ratios were tested and analyzed. Furthermore, based on test results, the optimal proportion scheme and heat storage/release temperature cycle range of CPB added with CEV was comprehensively determined. This study can provide more options for SSPCM applied to the deep mine environment, and provide a theoretical basis for the collaborative optimization of mechanical and thermal properties of CPB with SSPCM.

2. Experimental

2.1. Materials

In this experiment, anhydrous calcium chloride (CaCl_2) from Sinopharm Chemical Reagent Co., Ltd. (Shanghai, China) was used to prepare CEV, and strontium chloride hexahydrate ($\text{SrCl}_2 \cdot 6\text{H}_2\text{O}$, AR) from Xilong Scientific Co., Ltd. (Guangdong, China) was selected as an excellent nucleating agent to reduce the supercooling of $\text{CaCl}_2 \cdot 6\text{H}_2\text{O}$ [10]. Tailings were supplied by a gold mine in Meixian Country, Shaanxi, China. The chemical composition and particle size distribution of tailings was tested by an X-ray fluorescence spectrometer and a laser particle size scanner, and the results are shown in Table S1 and Fig. S1, respectively. Expanded vermiculite (20–40 mesh) was purchased from JingHang Mine Co., Ltd. (Hebei, China), and its particle size distribution curve is shown in Fig. S2. Portland cement (P.O 42.5), as the binder of CPB, was based on China's cement strength classification (GB175-2007-Portland cement), and its main chemical composition is given in Table S2. Tap water was used to mix the tailings, CEV, and cement to obtain CPB slurry.

2.2. Preparation

The 102.8 g of CaCl_2 and 4.06 g (2wt%) of $\text{SrCl}_2 \cdot 6\text{H}_2\text{O}$ were put into 100 g distilled water and stirred until completely dissolved, and then stored in the freezer. The expanded vermiculite dried at 105°C for 24 h was put into the melted $\text{CaCl}_2 \cdot 6\text{H}_2\text{O}$ in a 50°C oven. The expanded vermiculite as porous carrier material can alleviate the influence of PCM liquefaction on the UCS of CPB. The composites were stirred for 5 min to make expanded vermiculite evenly distributed in the melted $\text{CaCl}_2 \cdot 6\text{H}_2\text{O}$, and then put into a 50°C oven for 4 h. Excess liquid $\text{CaCl}_2 \cdot 6\text{H}_2\text{O}$ was filtered out with filter paper, and CEV was obtained finally. The leakage test was as follows: the obtained CEV was put into a 50°C oven, and the filter paper was replaced until there was no liquid trace on the filter paper and the mass change of CEV was less than 1%. The prepared CEV was stored in the freezer. The preparation process of CEV is shown in Fig. S3.

The CEV prepared above was used to replace part of the tailings by direct addition method to prepare the CPB specimens with slurry content of 70wt%. Firstly, a certain quality of cement, tailings, and CEV were put into the stirring pot for premixing. After that, a certain quality of tap water was put into the stirring pot, and then the automatic mixing mode of the cement mortar stirrer was open. When the mixing was over, the CPB slurry was poured into the cylindrical standard mold (diameter, $d = 50$ mm; height, $h = 100$ mm) with the inner surface pre-coated with mineral oil and cured for 24 h, and then the mold was removed. Formed specimens were put into hws-80 model standard curing box (temperature of $(20 \pm 2)^\circ\text{C}$, humidity of $(95 \pm 1)\%$) for 28 d. The proportion schemes of CPB are shown in Table 1. The preparation process and test flow of CPB are shown in Fig. 1.

Table 1. Proportion schemes of CPB

Group	Cement– tailing ratio	Ratio of CEV replacing tailings / %	Cement / g	Tailings / g	CEV / g
A0		0		280.0	0.0
A3		3		271.6	8.4
A6	1:4	6	70	263.2	16.8
A9		9		254.8	25.2
A12		12		246.4	33.6
B0		0		300.0	0.0
B3		3		291.0	9.0
B6	1:6	6	50	282.0	18.0
B9		9		273.0	27.0
B12		12		264.0	36.0
C0		0		311.0	0.0
C3		3		301.7	9.3
C6	1:8	6	39	292.3	18.7
C9		9		283.0	28.0
C12		12		273.7	37.3

Note: The cement–tailing ratio and slurry content were selected according to the conventional proportion in mining industry. The addition ratio of CEV was selected by referring to the addition of phase change materials in building walls [30] and combining with our previous research [31].

2.3. Test methods

The phase change enthalpy and specific heat capacity were tested by differential scanning calorimetry (DSC, DSC250, TA Instrument Inc., USA). The test procedure of DSC was as follows: 8–10 mg of specimens were sealed in an aluminum pan, and the test was conducted at a ramping rate of 3°C/min under N₂ gas atmosphere over the temperature range of 5–50°C. The thermal conductivity of specimens was tested by the transient plane source method using a thermal constant analyzer (TPS2500S, Hot Disk Inc., Sweden) with the test range of 0.005–500 W/(m·°C). In this test, two disc-shaped specimens with diameter of 50 mm and thickness of 10 mm were polished with 120 meshes coarse sandpaper firstly, and then were polished with 400 meshes

medium-grained sandpaper and 1000 meshes fine sandpaper successively to ensure the smoothness of contact surfaces between two specimens where the probe was placed. The UCS of specimens was tested by MTS electronic universal testing machine (C43.504, MTS Systems Co., Ltd, USA). The test stress rate was 0.500 MPa/s, the test strain rate was 0.0001 s⁻¹, the test speed was 1.000 mm/min, and the test temperature was 20°C. The microscopic morphology of CPB with a magnification of 500× was tested with a scanning electron microscope (SEM, JSM-6460LV JEOL, USA), and the porosity of CPB can be obtained by quantitative analysis of SEM images by ImageJ.

The maximum encapsulation capacity ($W\%$) can be calculated by Eqs. (1) and (2) [32–33]. Then, the calculation result of Eq. (1) on the maximum encapsulation capacity of expanded vermiculite for CaCl₂·6H₂O is verified by Eq. (2). If the calculation results of Eqs. (1) and (2) are close, the maximum encapsulation capacity can be determined.

$$W\% = \frac{m_{\text{CEV}} - m_{\text{EV}}}{m_{\text{CEV}}} \quad (1)$$

$$W\% = \frac{L_{\text{CEV}}}{L_{\text{CaCl}_2 \cdot 6\text{H}_2\text{O}}} \quad (2)$$

where m_{CEV} is the mass of prepared CEV, g; m_{EV} is the mass of expanded vermiculite before atmospheric impregnation, g; L_{CEV} is the latent heat of CEV, J/g; $L_{\text{CaCl}_2 \cdot 6\text{H}_2\text{O}}$ is the latent heat of CaCl₂·6H₂O, J/g.

When the temperature of SSPCM is in the phase change temperature range, the CPB added with SSPCM will accumulate heat in the form of latent heat. Therefore, it is necessary to use the effective specific heat capacity to represent the heat storage capacity of CPB in the phase change temperature range, and the larger the effective specific heat capacity of CPB in the phase change temperature range, the stronger the latent heat storage capacity of CPB. The effective specific heat capacity can be considered as the average specific heat capacity of the CPB added with CEV in the phase change temperature range, as shown in Fig. S4, which can be calculated by Eq. (3) [34]:



Fig. 1. Preparation process (a) and test flow (b) of CPB.

$$c_{ef} = \frac{\Delta h}{t_{max} - t_{min}} \quad (3)$$

where c_{ef} is the effective specific heat capacity of the CPB with CEV, $J/(g \cdot ^\circ C)$; Δh is the effective specific enthalpy of CPB with CEV at the fluctuation interval of phase change temperature, J/g ; t_{max} and t_{min} are maximum and minimum phase change temperature fluctuations, $^\circ C$.

3. Results and discussion

3.1. Thermal performance and the maximum encapsulation capacity of CEV

Fig. 2 shows that the trends of exothermic peaks and endothermic peaks for DSC curves of $CaCl_2 \cdot 6H_2O$ and CEV are basically the same, which indicates that expanded vermiculite can adsorb $CaCl_2 \cdot 6H_2O$ by atmospheric impregnation method. It can be seen from Table 2 that melting and solidifying temperatures of CEV are $30.20^\circ C$ and $22.07^\circ C$, which are similar to those of $CaCl_2 \cdot 6H_2O$, and the melting and solidifying enthalpies of CEV are $98.87 J/g$ and $97.56 J/g$, respectively. Therefore, the CEV prepared in this paper has good heat storage/release performance.

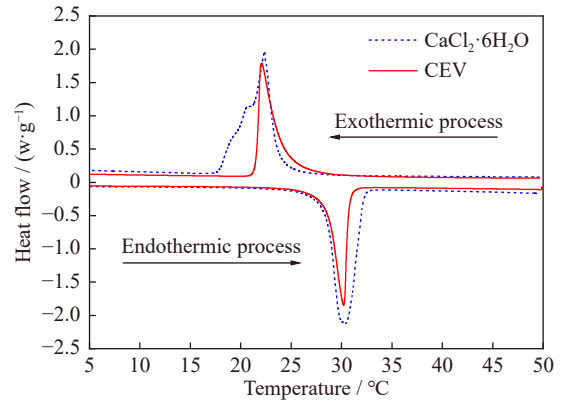


Fig. 2. DSC curves of $CaCl_2 \cdot 6H_2O$ and CEV.

It can be seen from Table 3 that the maximum encapsulation capacity calculated by Eq. (1) is basically the same with that calculated by Eq. (2), so it can be determined that the maximum encapsulation capacity is about 60%. In the process of preparing CEV, the leakage test was carried out repeatedly, so it can also be confirmed that the layered porous structure of expanded vermiculite can adsorb $CaCl_2 \cdot 6H_2O$ well.

Table 2. Thermal performance parameters of $CaCl_2 \cdot 6H_2O$ and CEV

Sample	Melting process		Solidifying process	
	Melting temperature / $^\circ C$	Latent heat / ($J \cdot g^{-1}$)	Solidifying temperature / $^\circ C$	Latent heat / ($J \cdot g^{-1}$)
$CaCl_2 \cdot 6H_2O$	30.35	163.59	22.35	162.87
CEV	30.20	98.87	22.07	97.56

Table 3. Maximum encapsulation capacity of CEV

Calculation basis	Test results	Maximum encapsulation capacity / %
Eq. (1)	$m_{EV} = 1.00 g, m_{CEV} = 2.55 g$	60.78
Eq. (2)	$L_{CEV} = 98.87 J/g, L_{CaCl_2 \cdot 6H_2O} = 163.59 J/g$	60.44

3.2. Analysis of influencing factors for specific heat capacity of CPB

3.2.1. cement–tailing ratio on specific heat capacity of CPB

Fig. 3 shows that the specific heat capacity of CPB increases linearly with the increase of temperature. When the temperature increases from 10 to $50^\circ C$, for CPB with cement–tailing ratio of 1:4, 1:6, and 1:8, the specific heat capacity increases from 1.100 to $1.153 J/(g \cdot ^\circ C)$, from 1.023 to $1.081 J/(g \cdot ^\circ C)$, and from 0.942 to $0.988 J/(g \cdot ^\circ C)$, respectively, with increase by about 4.54%, 5.44%, and 4.67% successively. The average growth rate is 4.88%. In addition, Fig. 3 also shows that the specific heat capacity decreases accordingly with the decrease of cement–tailing ratio. When the temperature is $20^\circ C$, as the cement–tailing ratio decreases from 1:4 to 1:6, and then to 1:8, the specific heat capacity decreases from 1.114 to $1.039 J/(g \cdot ^\circ C)$, and then to $0.954 J/(g \cdot ^\circ C)$, with decrease by 6.75% and 8.22% successively. According to the analysis, with the decrease of cement–tailing ratio, the cement content is decreased, the gel generated by hydration reaction is reduced, and the cementitious de-

gree of the tailings-based CPB is also reduced accordingly. In tailings-based CPB, the amount of gel produced is one of the key factors in the compactness of CPB [35], so the internal structure of CPB formed by curing has more pores and the specific heat capacity is smaller. Therefore, the sensible heat

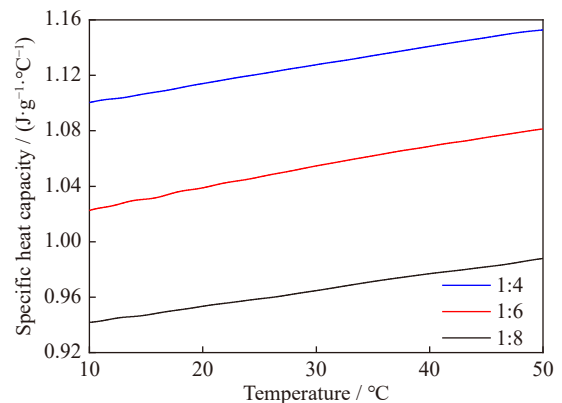


Fig. 3. Specific heat capacity with temperature for CPB at different cement-tailing ratios.

storage capacity of CPB can be improved by the increase of cement–tailing ratio.

3.2.2. CEV addition ratio on specific heat capacity of CPB

Fig. 4 and Fig. S5 show the specific heat capacity with temperature for CPB with different CEV addition ratios. Compared to the linear increase in specific heat capacity with temperature for CPB without CEV addition in Fig. 3, Fig. 4 shows that no matter how many ratios of CEV is added, the specific heat capacity has a great jump when the temperature reaches the phase change temperature range of the added CEV. According to the analysis, when CEV is added to CPB, as the temperature rises to the phase change temperature of $\text{CaCl}_2 \cdot 6\text{H}_2\text{O}$, the $\text{CaCl}_2 \cdot 6\text{H}_2\text{O}$ absorbs heat and transforms from solid to liquid, resulting in phase change latent heat storage. With the temperature continuing to rise, $\text{CaCl}_2 \cdot 6\text{H}_2\text{O}$ is completely transformed into liquid, and the phase change latent heat storage is completed at this time [36]. Therefore, the specific heat capacity of CPB with CEV added has a big jump.

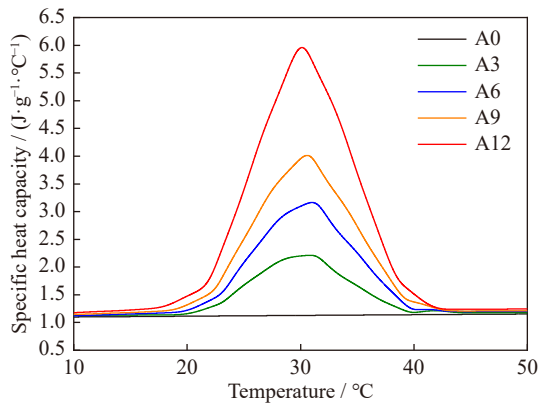


Fig. 4. Specific heat capacity of CPB with temperature under different CEV addition ratios with cement-tailing ratio of 1:4.

3.2.3. CEV addition ratio on specific heat capacity of CPB at phase change temperature range

It can be seen from Fig. 4 that CPB added with CEV presents a peak around the CEV phase change temperature of 20–40°C, so the concept of effective specific heat capacity is considered to analyze the latent heat storage capacity of CPB added with CEV. Fig. 5 shows that the effective specific heat capacity increases obviously with the increase of CEV addition ratio. When CPB is at the phase change temperature range and the cement–tailing ratio is 1:6, the effective specific heat capacity is 1.737, 2.189, 2.678, and 3.612 $\text{J}/(\text{g} \cdot ^\circ\text{C})$ respectively for 3%, 6%, 9%, and 12% CEV added, with increase by 64.80%, 107.58%, 154.01%, and 242.57% successively compared with that without CEV (1.054 $\text{J}/(\text{g} \cdot ^\circ\text{C})$). In the phase change temperature range, the effective specific heat capacity of CPB can significantly be increased by adding CEV. According to the analysis, with the increase of the ratio of CEV added to the CPB, more CEV undergoes phase change latent heat, which can stores more heat due to the properties of SSPCM [15,37]. At this time, the increase of specific heat capacity of CPB mainly depends on the latent heat stored by CEV. Obviously, the increase of effective spe-

cific heat capacity is beneficial to the thermal storage of CPB in phase change temperature range. Compared with the research of Jin *et al.* [38], the specific heat capacity of CPB with 12% CEV prepared in this paper can be increased by 2.25 times in the phase change temperature range, which has higher heat storage capacity.

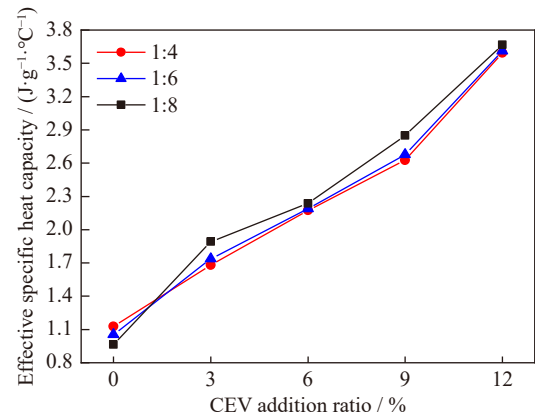


Fig. 5. Effective specific heat capacity of CPB with different CEV addition ratios at the phase change temperature range.

Fig. 5 also shows that the effective specific heat capacity of CPB increases with the decrease of cement–tailing ratio at the same CEV addition ratio, which is contrary to the law that the specific heat capacity of CPB without CEV decreases with the decrease of cement-sand ratio, so the specific heat capacity of CPB with 3% CEV is different from that of CPB without CEV. According to the analysis, with the decrease of cement–tailing ratio, the tailings content is relatively increased, so the addition of CEV instead of tailings will be correspondingly increased. At this time, the increase in the specific heat capacity of CPB is mainly due to the latent heat storage of CEV, while the increase in sensible heat capacity could be negligible with the increase of cement–tailing ratio in the case of latent heat storage occurring in CEV.

3.2.4. CEV addition ratio on specific heat capacity of CPB at non-phase change temperature

Fig. 6 shows that the specific heat capacity of CPB increases with the increase of CEV addition ratio, but the degree of increase is smaller. When the temperature is 15°C, at

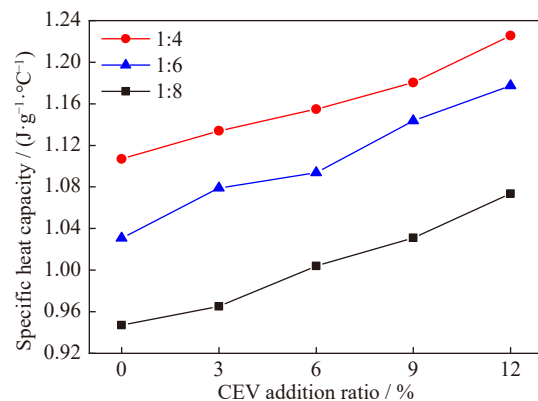


Fig. 6. Specific heat capacity of CPB with different CEV addition ratios at non-phase change temperature.

the cement–tailing ratio of 1:6, the specific heat capacities of CPB are 1.079, 1.094, 1.144, and 1.178 J/(g·°C) respectively for 3%, 6%, 9%, and 12% CEV added, which are increased by 4.69%, 6.11%, 10.95%, and 14.24% successively compared with that without CEV (the value is 1.031 J/(g·°C)). According to the analysis, the specific heat capacity of CEV prepared in this experiment can reach 1.583 J/(g·°C) when it does not reach the phase change temperature (15°C), thus it can be seen that the specific heat capacity of the whole CPB can be improved by adding CEV with high specific heat capacity, namely, the addition of CEV increases the sensible heat storage capacity of CPB to a certain extent.

3.3. Analysis of influencing factors for thermal conductivity of CPB

3.3.1. cement–tailing ratio on thermal conductivity of CPB

Fig. 7 shows that thermal conductivity decreases accordingly with the decrease of cement–tailing ratio. As the cement–tailing ratio decreases from 1:4 to 1:6, and then to 1:8, the thermal conductivity decreases from 0.834 to 0.717 W/(m·°C), and then to 0.622 W/(m·°C), which are decreased by 14.02% and 13.28% successively. According to the analysis, the cement plays an important role on the cementitious effect of CPB. The less the cement content, the worse the cementitious effect of CPB, and the more and larger the internal pores of CPB [31]. The pores are filled with air and the thermal conductivity of the air (0.024 W/(m·°C)) is relatively low [39], so the thermal conductivity decreases with the decrease of cement–tailing ratio.

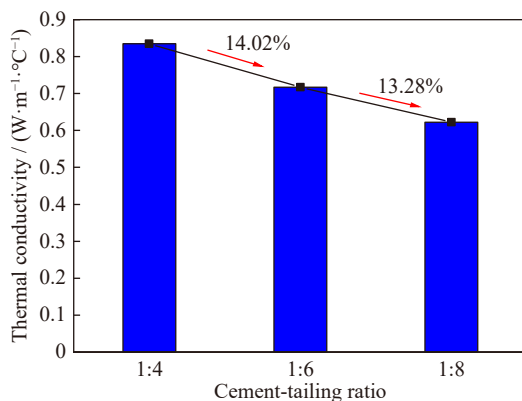


Fig. 7. Thermal conductivity of CPB without CEV at different cement–tailing ratios.

3.3.2. CEV addition ratio on thermal conductivity of CPB

Fig. 8 shows that the thermal conductivity of CPB decreases accordingly with the increase of CEV addition ratio. At the cement–tailing ratio of 1:6, the thermal conductivity values of CPB are 0.679, 0.632, 0.621, and 0.600 W/(m·°C) respectively for 3%, 6%, 9%, and 12% CEV added, which are decreased by 5.39%, 11.88%, 13.49%, and 16.35% successively compared with that without CEV (the value is 0.717 W/(m·°C)). The thermal conductivity of CPB decreases with the increase of CEV addition ratio, but the decrease degree has no obvious rule. According to the analysis, with the increase of CEV addition ratio, there are more pores

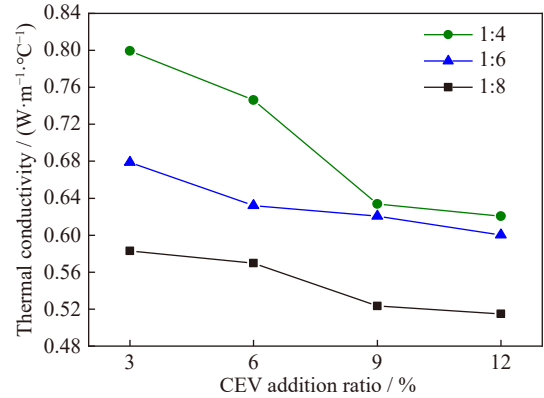


Fig. 8. Thermal conductivity of CPB with different CEV addition ratios.

in CPB, and expanded vermiculite, as a porous carrier material in CEV, has a large number of layered pores inside [40]. In Section 3.1, it is found that the maximum encapsulation capacity is about 60%, so there are still some layered pores which are not filled with CaCl₂·6H₂O, resulting in lower thermal conductivity of the SSPCM [9,41]. Under the combined action of the above two factors, the thermal conductivity will decrease with the increase of CEV addition ratio. The improvement of thermal conductivity for CPB added with SSPCM will become an important research direction of backfill technology in the future. On the one hand, high thermal conductivity materials, such as waste metal dross during the production process, can be added to CPB to make up for the reduction of thermal conductivity caused by the addition of SSPCM. On the other hand, a small amount of nano-metal can be added in the process of preparing SSPCM to fill the pores of the porous carrier material and reduce the pores, thereby increasing the thermal conductivity of SSPCM itself.

3.3.3. Temperature on thermal conductivity of CPB

Fig. 9 shows that the thermal conductivity of CPB is positively correlated with temperature. When the temperatures are 20, 30, and 40°C, the thermal conductivities of CPB without CEV are 0.717, 0.736, and 0.752 W/(m·°C), and the thermal conductivities of specimens with 6% and 12% CEV added are 0.632, 0.641, and 0.657 W/(m·°C) and 0.600, 0.616, and 0.633 W/(m·°C). When the temperature increases from 20 to

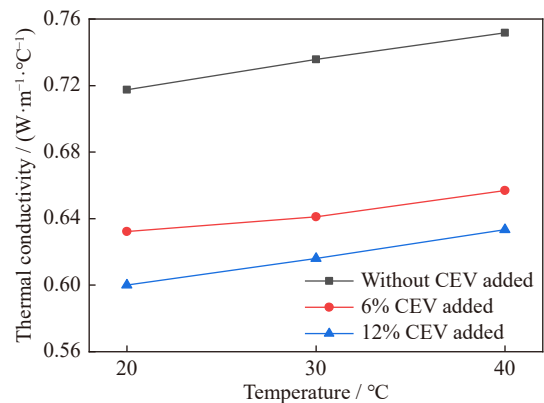


Fig. 9. Thermal conductivity of CPB with different temperatures at cement–tailing ratio of 1:6.

40°C, the thermal conductivity of CPB without CEV, with 6% CEV, and 12% CEV increases by 4.78%, 3.91%, and 5.53%, respectively. According to the analysis, the rise of temperature will accelerate the thermal movement of molecules in CPB, and promote the heat conduction of solid aggregate and the heat convection of air in the pores of CPB and CEV; therefore, the thermal conductivity of CPB increases with the increase of temperature.

3.4. Analysis of influencing factors for UCS of CPB

3.4.1. cement-tailing ratio on UCS of CPB

Fig. 10 shows that the UCS of CPB decreases accordingly with the decrease of cement-tailing ratio. As the cement-tailing ratio decreases from 1:4 to 1:6, and then to 1:8, the UCS of CPB without CEV decreases from 3.20 to 1.75 MPa, and then to 1.23 MPa, which are decreased by 45.26% and 29.81% successively. According to the analysis, with the decrease of cement-tailing ratio, the cement content with cementitious effect is decreased. The worse the cementitious effect, the more and larger the internal pores in CPB [42–43], which leads to the decrease of UCS of CPB with decreasing cement-tailing ratio.

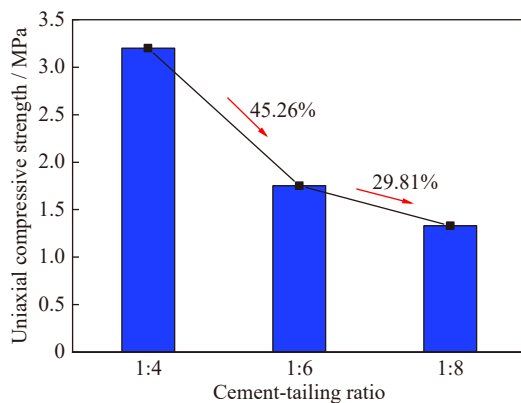


Fig. 10. UCS of CPB without CEV at different cement-tailing ratios.

Fig. 11 shows that there is also a law that the UCS decreases with the decrease of cement-tailing ratio for CPB with CEV added. As the cement-tailing ratio decreases from 1:4 to 1:6, and then to 1:8, the UCS of CPB with 3% CEV added decreases from 2.38 to 1.47 MPa, and then to 1.11 MPa, which are decreased by 38.01% and 24.44% successively. The figure also shows that the UCS values of CPB with 3% CEV added decrease by 25.73%, 15.88%, and 16.38% respectively for cement-tailing ratios of 1:4, 1:6, and 1:8 compared with that without CEV. It can be seen that the addition of CEV obviously decreases the UCS of CPB. According to the analysis, the physical properties of CEV itself determine that its strength is lower than that of common CPB [33,44]. Although expanded vermiculite has absorbed enough $\text{CaCl}_2 \cdot 6\text{H}_2\text{O}$, there are still pores inside it, and the addition of CEV to CPB will also cause extra pores, which further decreases the UCS of CPB.

3.4.2. CEV addition ratio on UCS of CPB

Fig. 12 shows that the UCS of CPB decreases accordingly

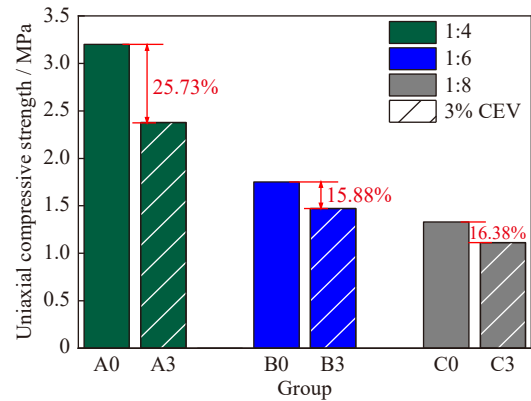


Fig. 11. UCS of CPB with 3% CEV added.

with the increase of CEV addition ratio. At the cement-tailing ratio of 1:6, the UCS of specimens are 1.47, 1.39, 1.28, and 1.24 MPa respectively for 3%, 6%, 9%, and 12% CEV added, which are decreased by 15.88%, 20.73%, 26.84%, and 29.47% successively compared with that without CEV (the value is 1.75 MPa). According to the analysis, the addition of more CEV will accelerate the formation of internal pores, so the UCS of CPB decreases with the increase of CEV addition ratio [45]. Comparing the UCS of CPB with the same CEV addition ratio, it can be seen that the UCS increases with the increase of cement-tailing ratio, so the increase of cement-tailing ratio can properly improve the weakening effect of CEV addition on UCS of CPB.

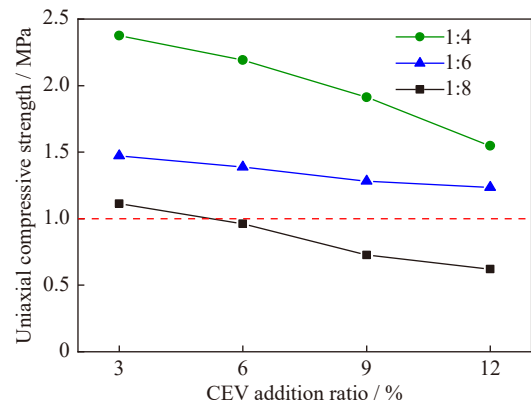


Fig. 12. UCS of CPB with different CEV addition ratios.

3.5. Relationship between porosity and properties of CPB

As shown in Fig. 13 and Fig. 14, the UCS and thermal conductivity of CPB are negatively correlated with porosity, and the porosity also increases with the decrease of cement-tailing ratio and with the increase of CEV addition ratio. The UCS and thermal conductivity of CPB are non-linearly proportional to the porosity at different cement-tailing ratios, however, the UCS and thermal conductivity of CPB are linearly proportional to the porosity at different CEV addition ratios. When considering the relationship between porosity and specific heat capacity, CPB with lower cement-tailing ratio without CEV addition is interfered by

porosity. However, the increase in specific heat capacity of CPB with added CEV is mainly due to CEV, so the increase in porosity and consequently the decrease in specific heat capacity due to the addition of CEV is negligible in the face of the increase in specific heat capacity due to heat storage by CEV. The microscopic morphology (porosity) of CPB is of great significance to explain the mechanical and thermal properties at different cement–tailing ratios and different CEV addition ratios.

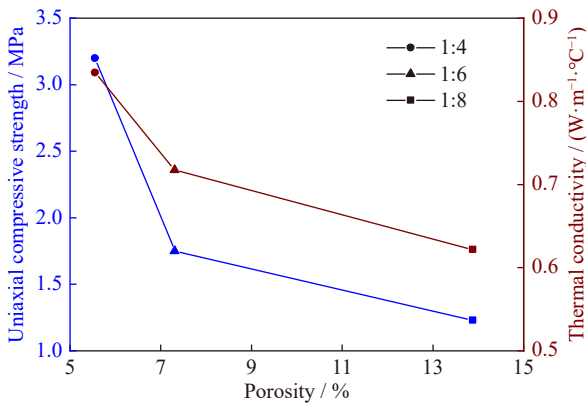


Fig. 13. Relationship between porosity and UCS and thermal conductivity with different cement-tailing ratios.

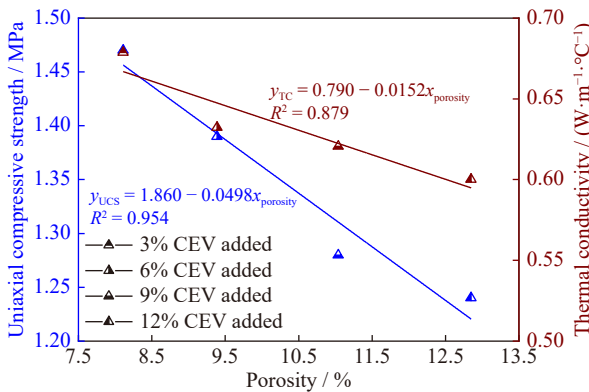


Fig. 14. Relationship between porosity and UCS and thermal conductivity with different CEV addition ratios and cement-tailing ratio of 1:6.

3.6. Comprehensive analysis of test results of CPB

According to the above analysis, considering proportion schemes of CPB based on different cement–tailing ratios and different CEV addition ratios, it is necessary to give priority to meet the mechanical properties of CPB required by the backfill mining technology, and then consider its better thermal properties and less cost price.

For metal ore backfill mining, the 28-days UCS of CPB must be greater than 1.0 MPa [46]. As shown in Fig. 12, the three proportion schemes (cement–tailing ratio is 1:8 and 6%, 9%, and 12% of CEV are added) should be discarded for metal ore backfill mining. Therefore, when considering the thermal properties, the case of adding CEV for cement–tailing ratios of 1:4 and 1:6 is only considered. To meet the high heat storage capacity of CPB needed by heat storage backfill

technology, it is necessary to select the proportion schemes from high-added CEV. Fig. 15 shows that considering the thermal conductivity, when the cement–tailing ratios are 1:4 and 1:6, the thermal conductivities of CPB with 9% and 12% CEV differ only 2.09% and 3.42%, respectively. Considering the specific heat capacity, it can be found that when the cement–tailing ratios are 1:4 and 1:6, the specific heat capacities of CPB with 9% CEV and 12% CEV are not much different in the phase change temperature range and the non-phase change temperature. However, compared with CPB added with 9% CEV, the latent heat storage capacity and sensible heat storage capacity of CPB with 12% CEV are at least 34.86% and 2.97% higher, respectively. Moreover, the latent heat storage has higher heat density and higher growth rate (34.86%), which should be considered as the leading index of heat storage performance. The cement consumption has a great influence on the cost and economic performance of CPB, and a slight reduction in cement will lead to substantial savings in the operating costs of CPB plants [47]. Meantime, the addition of CEV increases the initial investment of CPB, but it still has a good economic efficiency in the process of long-term heat extraction [48]. Therefore, the CPB with the CEV addition ratio of 12% and with the cement–tailing ratio of 1:6 has higher heat storage capacity and meets the mechanical properties of CPB, combined with the cost control considerations, and this proportion scheme of CPB is recommended.

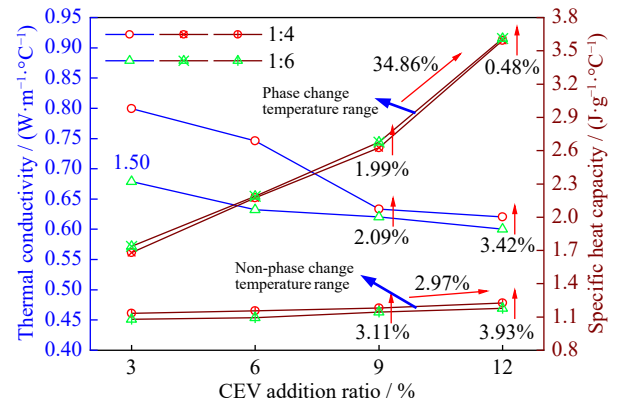


Fig. 15. Comprehensive analysis of CPB with cement-tailing ratios of 1:4 and 1:6.

In the process of thermal performance analysis, it is also found that, as shown in Fig. 4, the specific heat capacity of CPB with CEV addition has a large increase in the range of 20–40°C, and the phase change process of CEV can be used for latent heat storage. Fig. 15 shows that the addition of CEV can not only increase the sensible heat storage capacity of CPB, but also increase the latent heat storage capacity of CPB. Fig. 9 shows that the thermal conductivity of CPB increases with the temperature in the range of 20–40°C. Therefore, based on the thermal performance test results, it is recommended that the heat storage/release temperature cycle range of CPB with CEV added is from 20 to 40°C in this study.

4. Conclusions

In this paper, the CEV was prepared by atmospheric impregnation method, and the CPB specimens with different cement–tailing ratios and different CEV addition ratios were prepared by direct addition method. The thermal performance of CEV and the thermal properties and mechanical properties of CPB specimens were tested. The main conclusions are as follows:

(1) The melting and solidification enthalpies of CEV can reach 98.87 J/g and 97.56 J/g, respectively, which has good heat storage/heat release performance.

(2) The specific heat capacity of CPB without CEV increases with the increase of temperature, and the average growth rate is 4.88% when the temperature increases from 10 to 50°C. The specific heat capacity of CPB without CEV decreases with the decrease of the cement–tailing ratio. With the increase of CEV addition ratio, the specific heat capacity of CPB increases correspondingly, and its sensible heat storage capacity and latent heat storage capacity can be increased by at least 10.74% and 218.97% respectively after adding 12% CEV.

(3) The thermal conductivity of CPB without CEV decreases with the decrease of the cement–tailing ratio, as the cement–tailing ratio decreases from 1:4 to 1:6, and then to 1:8, the thermal conductivity decreases by 14.02% and 13.28% successively. The thermal conductivity of CPB decreases with the increase of CEV addition ratio, but the decrease degree has no obvious rule. In addition, the thermal conductivity of CPB increases with the increase of temperature.

(4) The UCS of CPB without CEV decreases with the decrease of the cement–tailing ratio. In addition, the UCS of CPB decreases obviously with the increase of CEV addition ratio, and the UCS of CPB adding CEV decreases by 53.42% at most. However, the increase of cement–tailing ratio can properly improve the weakening effect of CEV addition on the UCS of CPB.

(5) The proportion scheme of CPB with the CEV addition ratio of 12% and with the cement–tailing ratio of 1:6 is recommended. Based on the thermal property test results, it is recommended that the heat storage/release temperature cycle range of CPB with CEV added is from 20 to 40°C.

Acknowledgements

This work was supported by the National Natural Science Foundation of China (Nos. 51974225, 51874229, 51674188, 51904224, and 51904225), the Shaanxi Innovative Talents Cultivate Program-New-star Plan of Science and Technology, China (No. 2018KJXX-083), the Natural Science Basic Research Plan of Shaanxi Province of China (Nos. 2018JM5161, 2018JQ5183, and 2019JM-074), the Scientific Research Program funded by the Shaanxi Provincial Education Department, China (No. 19JK0543), and the Outstanding Youth Science Fund of Xi'an University of Science and

Technology, China (No. 2018YQ2-01).

Conflict of Interest

There are no conflicts of interest for this work.

Supplementary Information

The online version contains supplementary material available at <https://doi.org/10.1007/s12613-022-2503-7>.

References

- [1] H.P. Xie, F. Gao, Y. Ju, *et al.*, Quantitative definition and investigation of deep mining, *J. China Coal Soc.*, 40(2015), No. 1, p. 1.
- [2] H.Y. Cheng, A.X. Wu, S.C. Wu, *et al.*, Research status and development trend of solid waste backfill in metal mines, *Chin. J. Eng.*, 44(2022), No. 1, p. 11.
- [3] Y. Dong, X.J. Liu, and H.L. Hou, Analysis of green mine evaluation index, *China Min. Mag.*, 29(2020), No. 12, p. 68.
- [4] L. Liu, J. Xin, B. Zhang, *et al.*, Basic theories and applied exploration of functional backfill in mines, *J. China Coal Soc.*, 43(2018), No. 7, p. 1811.
- [5] X.C. Hu, J. Banks, L.P. Wu, and W.V. Liu, Numerical modeling of a coaxial borehole heat exchanger to exploit geothermal energy from abandoned petroleum wells in Hinton, Alberta, *Renewable Energy*, 148(2020), p. 1110.
- [6] X.Y. Zhang, M. Zhao, L. Liu, *et al.*, Numerical simulation on heat storage performance of backfill body based on tube-in-tube heat exchanger, *Constr. Build. Mater.*, 265(2020), art. No. 120340.
- [7] D.V. Voronin, E. Ivanov, P. Gushchin, R. Fakhruddin, and V. Vinokurov, Clay composites for thermal energy storage: A review, *Molecules*, 25(2020), No. 7, art. No. 1504.
- [8] P.Z. Lv, C.Z. Liu, and Z.H. Rao, Review on clay mineral-based form-stable phase change materials: Preparation, characterization and applications, *Renewable Sustainable Energy Rev.*, 68(2017), p. 707.
- [9] Y. Deng, J.H. Li, T.T. Qian, W.M. Guan, and X. Wang, Polyethylene glycol/expanded vermiculite shape-stabilized composite phase change materials for thermal energy storage, *Mater. Sci. Forum*, 847(2016), p. 39.
- [10] L.L. Fu, Q.H. Wang, R.D. Ye, X.M. Fang, and Z.G. Zhang, A calcium chloride hexahydrate/expanded perlite composite with good heat storage and insulation properties for building energy conservation, *Renewable Energy*, 114(2017), p. 733.
- [11] W.B. Jia, C.M. Wang, T.J. Wang, Z.Y. Cai, and K. Chen, Preparation and performances of palmitic acid/diatomite form-stable composite phase change materials, *Int. J. Energy Res.*, 44(2020), No. 6, p. 4298.
- [12] Y. Deng, J.H. Li, and H.E. Nian, Expanded vermiculite: A promising natural encapsulation material of LiNO₃, NaNO₃, and KNO₃ phase change materials for medium-temperature thermal energy storage, *Adv. Eng. Mater.*, 20(2018), No. 8, art. No. 1800135.
- [13] W.M. Jia, J.H. Ji, M.Y. Zhang, X.J. Zhang, H.M. Cheng, and H.M. Dong, Research and engineering application of high temperature and thermal damage prevention in deep mines, *Coal Technol.*, 39(2020), No. 3, p. 88.
- [14] M. Wang, L. Liu, B. Zhang, *et al.*, Basic theory of cold load and storage functional backfill in mining, *J. China Coal Soc.*, 45(2020), No. 4, p. 1336.
- [15] Y.E. Milián, A. Gutiérrez, M. Grágeda, and S. Ushak, A review

- on encapsulation techniques for inorganic phase change materials and the influence on their thermophysical properties, *Renewable Sustainable Energy Rev.*, 73(2017), p. 983.
- [16] J. Xin, L. Liu, L.H. Xu, J.Y. Wang, P. Yang, and H.S. Qu, A preliminary study of aeolian sand-cement-modified gasification slag-paste backfill: Fluidity, microstructure, and leaching risks, *Sci. Total Environ.*, 830(2022), art. No. 154766.
- [17] N. Zhou, C.W. Dong, J.X. Zhang, G.H. Meng, and Q.Q. Cheng, Influences of mine water on the properties of construction and demolition waste-based cemented paste backfill, *Constr. Build. Mater.*, 313(2021), art. No. 125492.
- [18] N. Zhou, E.B. Du, J.X. Zhang, C.L. Zhu, and H.Q. Zhou, Mechanical properties improvement of sand-based cemented backfill body by adding glass fibers of different lengths and ratios, *Constr. Build. Mater.*, 280(2021), art. No. 122408.
- [19] Z.W. Du, S.J. Chen, S. Wang, R. Liu, D.H. Yao, and H.S. Mitri, Influence of binder types and temperatures on the mechanical properties and microstructure of cemented paste backfill, *Adv. Civ. Eng.*, 2021(2021), art. No. 6652176.
- [20] Y.Y. Tan, E. Davide, Y.C. Zhou, W.D. Song, and X. Meng, Long-term mechanical behavior and characteristics of cemented tailings backfill through impact loading, *Int. J. Miner. Metall. Mater.*, 27(2020), No. 2, p. 140.
- [21] Q. Zhou, J.H. Liu, A.X. Wu, and H.J. Wang, Early-age strength property improvement and stability analysis of unclassified tailing paste backfill materials, *Int. J. Miner. Metall. Mater.*, 27(2020), No. 9, p. 1191.
- [22] J. Wang, J.X. Fu, W.D. Song, Y.F. Zhang, and Y. Wang, Mechanical behavior, acoustic emission properties and damage evolution of cemented paste backfill considering structural feature, *Constr. Build. Mater.*, 261(2020), art. No. 119958.
- [23] Y.L. Shen, S.L. Liu, C. Zeng, et al., Experimental thermal study of a new PCM-concrete thermal storage block (PCM-CTSB), *Constr. Build. Mater.*, 293(2021), art. No. 123540.
- [24] M. Ren, X.D. Wen, X.J. Gao, and Y.S. Liu, Thermal and mechanical properties of ultra-high performance concrete incorporated with microencapsulated phase change material, *Constr. Build. Mater.*, 273(2021), art. No. 121714.
- [25] X. Sun, W.Y. Liao, A. Kumar, K.H. Khayat, Z.H. Tian, and H.Y. Ma, Multi-level modeling of thermal behavior of phase change material incorporated lightweight aggregate and concrete, *Cem. Concr. Compos.*, 122(2021), art. No. 104131.
- [26] A. Ilyas, M.Z. Ahad, M.A.Q.J. Durrani, and A. Naveed, Synthesis and characterization of PCM based insulated concrete for thermal energy storage, *Mater. Res. Express*, 8(2021), No. 7, art. No. 075503.
- [27] J. Chen, W.M. Zhang, X.J. Shi, C. Yao, and C.C. Kuai, Use of PEG/SiO₂ phase change composite to control porous asphalt concrete temperature, *Constr. Build. Mater.*, 245(2020), art. No. 118459.
- [28] A.L. Brooks, Y. Fang, Z.L. Shen, J.L. Wang, and H.Y. Zhou, Enabling high-strength cement-based materials for thermal energy storage via fly-ash cenosphere encapsulated phase change materials, *Cem. Concr. Compos.*, 120(2021), art. No. 104033.
- [29] E. Mohseni, W. Tang, K.H. Khayat, and H.Z. Cui, Thermal performance and corrosion resistance of structural-functional concrete made with inorganic PCM, *Constr. Build. Mater.*, 249(2020), art. No. 118768.
- [30] L. Zhu, F.N. Dang, Y. Xue, K. Jiao, and W.H. Ding, Multivariate analysis of effects of microencapsulated phase change materials on mechanical behaviors in light-weight aggregate concrete, *J. Build. Eng.*, 42(2021), art. No. 102783.
- [31] X.Y. Zhang, M.Y. Xu, L. Liu, et al., Experimental study on thermal and mechanical properties of cemented paste backfill with phase change material, *J. Mater. Res. Technol.*, 9(2020), No. 2, p. 2164.
- [32] X.G. Zhang, J.X. Qiao, W.Y. Zhang, et al., Thermal behavior of composite phase change materials based on polyethylene glycol and expanded vermiculite with modified porous carbon layer, *J. Mater. Sci.*, 53(2018), No. 18, p. 13067.
- [33] B.W. Xu, H.Y. Ma, Z.Y. Lu, and Z.J. Li, Paraffin/expanded vermiculite composite phase change material as aggregate for developing lightweight thermal energy storage cement-based composites, *Appl. Energy*, 160(2015), p. 358.
- [34] C. Chen, H.S. Ling, N. Yu, N. Li, M.X. Zhang, and Y. Li, Calculation method of heat storage coefficient of phase change material, *Acta Energetica Solaris Sin.*, 39(2018), No. 8, p. 2267.
- [35] L. Liu, P. Yang, C.C. Qi, B. Zhang, L.J. Guo, and K.I. Song, An experimental study on the early-age hydration kinetics of cemented paste backfill, *Constr. Build. Mater.*, 212(2019), p. 283.
- [36] H.W. Min, S. Kim, and H.S. Kim, Investigation on thermal and mechanical characteristics of concrete mixed with shape stabilized phase change material for mix design, *Constr. Build. Mater.*, 149(2017), p. 749.
- [37] X. Liu, J.H. Wu, T. Xian, and Y. Feng, Preparation and properties of CaCl₂-6H₂O/expanded graphite composite phase change materials, *J. Zhejiang Univ. (Eng. Sci.)*, 53(2019), No. 7, p. 1291.
- [38] A.B. Jin, Y. Ju, H. Sun, et al., Strength and thermal performance of phase change energy storage backfill, *J. Harbin Inst. Technol.*, 54(2022), No. 2, p. 81.
- [39] X.M. Zhang, T. Zhu, Q.S. An, Z.P. Ren, and F.M. Mei, *Heat Transfer*, 6th ed., China Architecture & Building Press, Beijing, 2014, p. 13.
- [40] H. Yang, W.H. Chen, X.F. Kong, and X. Rong, Fabrication, property characterization and thermal performance of composite phase change material plates based on tetradecanol-myristic acid binary eutectic mixture/expanded perlite and expanded vermiculite for building application, *J. Cent. South Univ.*, 26(2019), No. 9, p. 2578.
- [41] S.G. Jeong, S.J. Chang, S. Wi, et al., Energy efficient concrete with n-octadecane/xGnP SSPCM for energy conservation in infrastructure, *Constr. Build. Mater.*, 106(2016), p. 543.
- [42] N. Li, S.W. Lv, W. Wang, J. Guo, P. Jiang, and Y. Liu, Experimental investigations on the mechanical behavior of iron tailings powder with compound admixture of cement and nano-clay, *Constr. Build. Mater.*, 254(2020), art. No. 119259.
- [43] L. Cui and M. Fall, Mechanical and thermal properties of cemented tailings materials at early ages: Influence of initial temperature, curing stress and drainage conditions, *Constr. Build. Mater.*, 125(2016), p. 553.
- [44] W.X. Wu, W. Wu, and S.F. Wang, Form-stable and thermally induced flexible composite phase change material for thermal energy storage and thermal management applications, *Appl. Energy*, 236(2019), p. 10.
- [45] A. Adesina, P.O. Awoyera, A. Sivakrishna, K.R. Kumar, and R. Gobinath, Phase change materials in concrete: An overview of properties, *Mater. Today Proc.*, 27(2020), p. 391.
- [46] Y. Yang, A.H. Wu, and L.H. Yang, Experimental study on the properties of unclassified tailing paste, *Metal Mine*, 45(2016), No. 8, p. 185.
- [47] S.H. Yin, A.X. Wu, K.J. Hu, Y. Wang, and Y.K. Zhang, The effect of solid components on the rheological and mechanical properties of cemented paste backfill, *Miner. Eng.*, 35(2012), p. 61.
- [48] B. Zhang, P.Y. Xue, L. Liu, et al., Exploration on the method of ore deposit-geothermal energy synergetic mining in deep backfill mines, *J. China Coal Soc.*, 46(2021), No. 9, p. 2824.